ENSO-related precipitation variability in Central Chile: the role of large scale moisture transport.

Diego Campos[1], Roberto Rondanelli [2,3*]

1. Dirección Meteorológica de Chile
2. Departamento de Geofísica, Universidad de Chile
3. Centro de Ciencia del Clima y la Resiliencia, (CR)2

*Corresponding author: ronda@dgf.uchile.cl

Key Points:

- Moisture transport in the Southern Pacific is enhanced during the El Niño, between a large-scale tropical high and a subtropical low.
- The frequency of atmospheric rivers maximize in a region at around 110ºW and 25ºS consistent with an increase in transient eddies.
- The increased moisture transport is connected to longer-lasting and moister atmospheric rivers landfalling in Central Chile.

Abstract

Interannual variability of precipitation in Central Chile has long been associated with changes in the dry atmospheric dynamics of the Southern Pacific. This is due to the interaction between the extratropical storm track and the polar anticyclonic circulations established by the Pacific South American (PSA) teleconnection mode, which results from changes in tropical convection. Here, we show that an enhanced subtropical moisture transport during the warm ENSO phase leads to an increase in the frequency of atmospheric rivers, larger values of precipitable water, and heightened zonal integrated water vapor transport. This occurs in a region of the Southern Pacific situated between the tropical high and the subtropical low of the PSA mode. These increases in zonal water vapor transport result in greater precipitation and moister, long-lived atmospheric rivers making landfall in Central Chile

1. Introduction

The interannual variability of precipitation along the coast of the southeastern Pacific has long been studied, mainly focusing on the relationship between precipitation and sea surface temperature (SST) in the central equatorial Pacific. For several decades, we have known that warm anomalies in the central Pacific are connected to wetter conditions in Central Chile during the austral winter (El Niño years) (Pittock, 1980), whereas below-normal rainfall occurs when the subtropical anticyclone intensifies and moves poleward during the positive phase of the Southern Oscillation, (La Niña years) (Aceituno, 1988; Rubin, 1955). Both the variability of the central equatorial Pacific SST and the intensity and location of the subtropical anticyclone, are driven by ENSO at the interannual scales, explaining about 40% of the variance of rainfall in Central Chile (Garreaud et al., 2017).

Regarding the physical mechanism behind this relationship, literature has greatly emphasized the dry dynamic mechanisms. For instance, (Quinn & Neal, 1983) attributed the increase in precipitation to the increase in SST along the western coast of South America during positive ENSO years, thereby inducing a weakening of the subtropical anticyclone. However, as mentioned by (Rutllant, 2004), SST along the coast of Chile rarely gets over the lower threshold to trigger tropical deep convection in the present climate (27-28°C), as it is possible to observe on the coast of Peru during El Niño years. Therefore, the mechanism for the increase in precipitation in central Chile is not directly related to local sea surface warming.

The main winter storms in Central and Southern Chile during the warm phase of ENSO are associated with blocking highs embedded in a hemispheric circulation pattern of high latitudes with wave numbers 3 and 4 (Rutllant & Fuenzalida, 1991). The presence of blocking highs over the Amundsen-Bellingshausen Sea (90°W) during El Niño years occurs in association with a wave pattern extending from the equatorial Pacific poleward and eastward along the South Pacific, as a wave train of alternating highs and lows (Karoly, 1989; Montecinos & Aceituno, 2003; Rutllant & Fuenzalida, 1991), as described for the Northern Hemisphere by (Horel & Wallace, 1981) and known loosely in the literature as the Pacific South American teleconnection mode (e.g. Mo & Higgins, 1998).

Emphasis on the blocking high in the Amundsen-Bellingshausen region has resulted in the "dry-dynamics" explanation for the relationship between the positive ENSO phase and the wet anomalies in the Central Chile region, which can be summarized as follows. Anomalous deep convection in the Central Pacific, near the 3.4 El Niño region, triggers a Pacific South American teleconnection in the form of a Rossby wave train consisting of a tropical high, a subtropical low, and a blocking high located in the Amundsen-Bellingshausen region. This blocking high produces a split in the extratropical circulation near South America, generating cyclonic anomalies in the band between 30ºS-40ºS, diverting the extratropical storm track towards the subtropics, thereby increasing the frequency of storms in Central and Southern Chile. Examples of the "dry-dynamics" explanation of the influence of ENSO in Central Chile rainfall prevail in the literature. For instance, (Marques &

Rao, 1999) wrote about a case study during the winter of 1986: "*The increase of precipitation to the north of the blocking high was associated with the deflection of transient eddies to the north of the block*." (Rutllant, 2004) writes about the indirect mechanism that controls the increase in precipitation during El Niño years in Central Chile: "*blocking highs around 120ºW force the separation of the westerlies into two branches, one towards the subtropics and one towards the subpolar region, dragging with them the trajectories of the extratropical depressions and associated frontal systems*". A recent example of the dry dynamics view can be found in the review chapter by (Aceituno et al., 2021): "*El Niño leads to anticyclonic circulation anomalies over the Amundsen-Bellingshausen Sea. The stationary and quasi-barotropic nature of these high-pressure systems blocks the westerlies and associated polar-front jet stream, diverting the storm track toward subtropical latitudes*".

Here, we argue that this leading dry dynamical explanation is not entirely satisfactory, as it neglects the major role of moisture transport in explaining precipitation along the coast of Southwestern South America. Fig. 1a shows the distribution of precipitable water in the South Pacific during the winter months. The white solid line shows the mean position of the South Pacific Convergence Zone (e.g. Vincent, 1994), which can be seen as an extension of the large values of precipitable water typical of the warm pool region (60 to 30 mm at the southeastern tip of the region). One could extend the axis of the South Pacific convergence region towards South America, where values of precipitable water are relatively low —ranging from about 10 to 15 mm—. Despite the relatively low mean climatological values of PW, precipitation along Chile ranges from zero at about 20ºS to 1500 mm at around 40°S in the JJA period, as seen in Fig. 1b. South of 40ºS, in the Patagonian Ice fields, annual precipitation can reach extreme values, even higher than 10000 mm/year according to numerical models (Carrasco-Escaff et al., 2022).

Southern Patagonia, and in general, the western coast of South America, is a region with cold surface temperatures and, therefore, relatively low local availability of water vapor. How can these large precipitation accumulations —similar to the largest accumulations found within the tropics— arise in these relatively dry extratropical regions? On the one hand, the interaction between topography and a quasi-stationary westerly storm track induces frequent precipitation from extratropical storms. However, a major role is played by the transport of water along thousands of kilometers provided by atmospheric rivers (Guan & Waliser, 2015; Langhamer et al., 2018; Saavedra et al., 2020; Viale et al., 2018). Water vapor is transported from the Northwest towards Central and Southern Chile, which produces a water vapor "ridge" in the precipitable water vapor field, which is marked as a white dashed line in Fig. 1a. One could consider this dashed line as the natural extension of the South Pacific Convergence Zone towards South America, which manifests itself episodically through these water vapor transport events.

Although the importance of atmospheric rivers in precipitation in Central and Northern Chile during El Niño years has been previously recognized (Rutllant et al., 2023; e.g. Saavedra et al., 2020), there has been no attempt to describe the large-scale mechanisms that explain this relation, and in particular to reconcile the dry dynamical explanation with the apparent increase in frequency, intensity, and duration of ARs during the warm ENSO phase. Here, we show how ENSO modulates this moisture transport at the interannual scale, which is an essential —and mostly neglected— part of the explanation for the increase in rainfall in Central Chile during El Niño years.

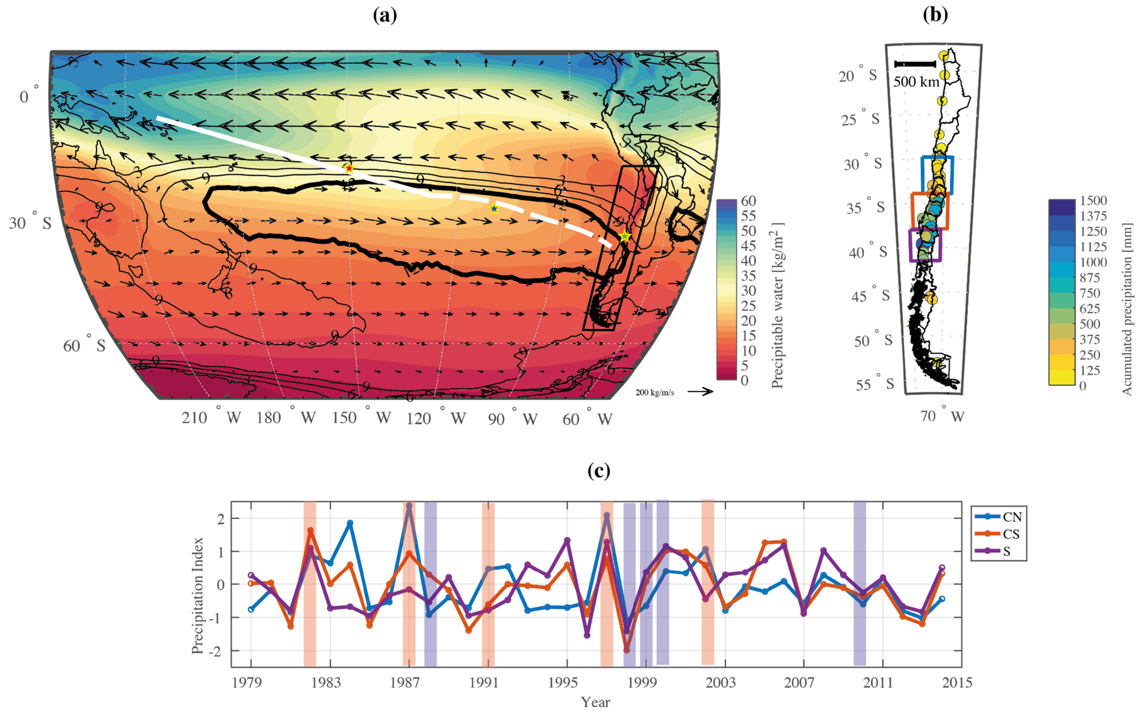

Figure 1: Winter climatology (JJA) for 1981-2010. (a) Composite of the mean values of PW in colors (kg/m2), IVT in vectors (kg/m/s), and frequency of ARs in contours (percent of the time). Thick line indicates 12%, and contours decrease every 2%. Thick white line shows the position and orientation of the SPCZ (Vincent, 1994), and the thick white dash line shows the PW ridge (see text). (b) Average accumulated precipitation in Chile (mm). (c) Time series of the precipitation index for the central-north (CN), central-south (CS), and southern (S) regions of Chile. The delimitation of each zone is shown in (b). Red (blue) line in (c) shows El Niño (La Niña) winters. Stars in (a) represent radiosonde launch locations in Tahiti (red), Easter Island (blue), and Santo Domingo (green).

2. Data

To categorize El Niño and La Niña, the Oceanic El Niño Index (ONI) was used between 1979 and 2014, obtained directly from CPC-NOAA (L'Heureux et al., 2013). A JJA (June, July, August) season was considered El Niño when the average ONI was higher than 0.5 and La Niña for an average ONI smaller than -0.5. Using these criteria, 5 El Niño and 5 La Niña years were obtained over the 36-year period (see Figure 1c).

Monthly precipitation, geopotential height, zonal and meridional wind, and specific humidity data were obtained from the ERA-Interim reanalysis (Dee et al., 2011). A monthly database of precipitable water PW (kg m^{-2}) and integrated transport of water vapor, IVT (kg m^{-1} s^{-1}), was built using the monthly values of wind and specific humidity integrated from 1000 hPa up to 100 hPa. Additionally, monthly outgoing longwave radiation data, OLR, were obtained from the NOAA Interpolated OLR database (Liebmann & Smith, 1996), and monthly streamfunction (at 300 hPa) was derived from monthly u and v data.

An ERA-Interim-derived global catalog was used to obtain the frequency of atmospheric rivers (Guan & Waliser, 2015). Seasonal frequencies for the JJA period were obtained from the sub-daily data, and climatological values were calculated using the 1981-2010 period. Daily frequencies of AR in central Chile were calculated by looking at the existence of conditions of ARs in each of the boxes (see Figure 1b) uninterrupted during a certain length of time using the sub-daily data and expressed in percentage of the time.

Daily and monthly data from 35 rain gauge stations covering continental Chile were obtained from Dirección Meteorológica de Chile (DMC) and Dirección General de Aguas (DGA). Three climatic zones were defined following (Montecinos & Aceituno, 2003): central-north (CN), central-south (CS), and south (S) (see Figure 1b). A wintertime (JJA) standardized precipitation index for each zone was calculated and presented in Figure 1c.

In order to obtain PW and IVT daily observations for the study period (1979-2014), data for the entire tropospheric column from regular 12 UTC radiosondes launches in Santo Domingo, Easter Island, and Tahiti was obtained from the University of Wyoming website (https://weather.uwyo.edu/upperair/sounding.html). For the case of Santo Domingo, prior to 1999, data from Quintero were used. See Figure 1a for locations.

3. Results

To illustrate the year-to-year covariance between precipitation in central-southern Chile and water vapor content and transport, we applied the linear correlation between the precipitation series for the CS zone and the data from ERA-Interim between 1979 and 2014 (data were detrended). Precipitation strongly correlates with IVT's zonal component (uIVT, zonal water vapor transport). A maximum positive correlation (~0.8) at the coast is slightly displaced to the north of the CS zone extending diagonally towards the Western Pacific, slowly decreasing in magnitude. A band of negative correlations centered is found at about 50 ºS with a maximum amplitude of ~ -0.8 (Fig. 2a). Precipitation and meridional water vapor transport (vIVT) are negatively correlated (r ~ -0.7), showing a more local pattern than the one observed for uIVT (Fig. 2b), that is, northerly flow along the coast is correlated with positive precipitation. Correlations between PW and rainfall, and especially between AR frequency and rainfall, are quite similar to the uIVT-rainfall, with slightly weaker correlations. The AR frequency and precipitation exhibit a maximum correlation of ~0.7 at the coast, and the PW-precipitation correlation shows two local maxima of ~ 0.6 at around 90ºW and 70ºW (Fig. 2c,d). Similar results are observed for CN and S zones (see Fig. S1 and S2).

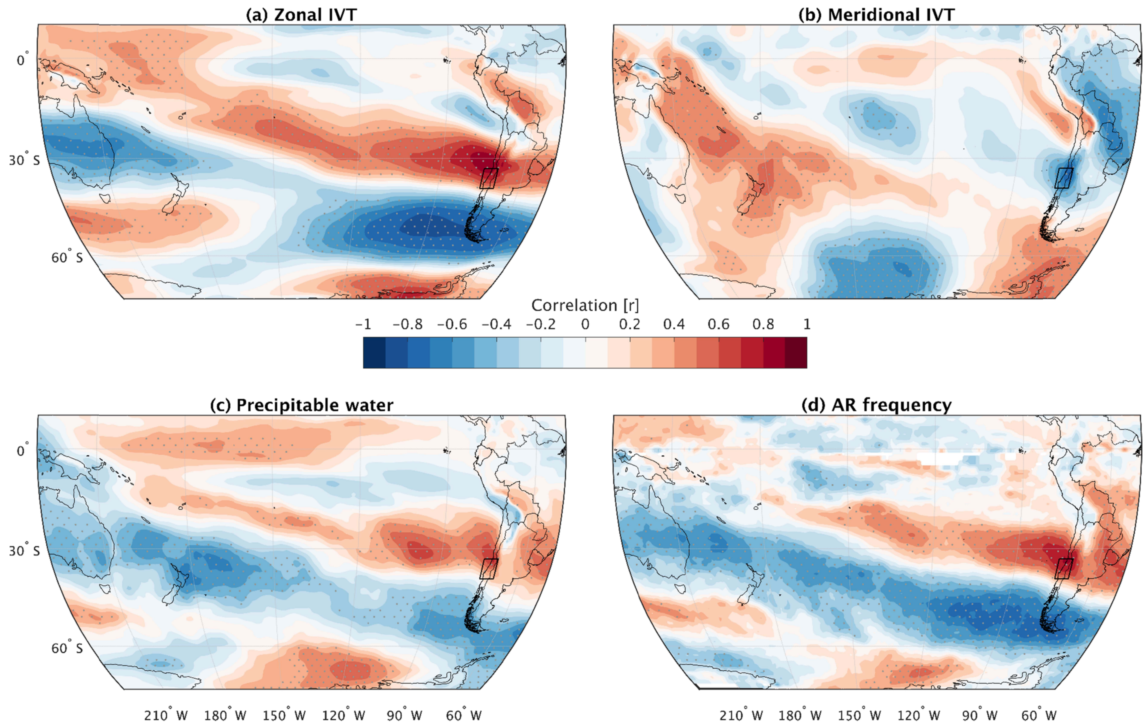

Figure 2: Composite of the interannual correlation (1979-2014) between the CS precipitation index and (a) zonal integrated water vapor transport uIVT, (b) meridional integrated water vapor transport vIVT, (c) PW, and (d) ARs frequency. Shaded area shows statistically significant correlations at the 95% level, according to a Monte Carlo test (n = 10000). Box over the map shows the location of the CS zone.

The spatial correlation pattern suggests that an increase in precipitation in central-southern Chile is associated with a higher frequency of atmospheric rivers in the diagonal from the tropical SouthWestern Pacific (20°S-150°W) towards central-southern Chile and a decrease in the frequency of water vapor transport and frequency of atmospheric rivers from Eastern Australia towards the Eastern Pacific, south of 45ºS. The higher frequency of atmospheric rivers is consistent with an increase in uIVT and PW from the Pacific and an increase in northerly moisture transport on the Chilean coast once the ARs make landfall (Barrett et al., 2009; Valenzuela & Garreaud, 2019; Viale et al., 2018).

The interannual variability of water vapor content and transport and its relationship with ENSO will now be explored (Fig. 3). For this purpose, correlations between ONI and data from ERA-Interim between 1979 and 2014 were calculated (both fields were detrended). The uIVT shows a positive and significant correlation with ONI (~0.7) in a strip that connects the Western tropical Pacific with the western coast of South America (the "extended" SPCZ region in Fig. 1a), similar to what is observed for PW and the AR frequency. An increase in the equatorial Pacific SST is associated with an increase in the zonal transport of water vapor from the Western tropical Pacific towards South America, together with an increase in water vapor content and the frequency of atmospheric rivers. On the other hand, vIVT is negatively correlated with ONI offshore South America in an area centered between 30°S and 100°W. Also noticeable are the increase in uIVT in the equatorial Western Pacific (a consequence of the relaxation of the trade winds, Fig. 3a) and a widespread increase in PW in the equatorial Pacific (Fig. 3c) consistent with the higher SSTs along the equator during the warm phase of ENSO.

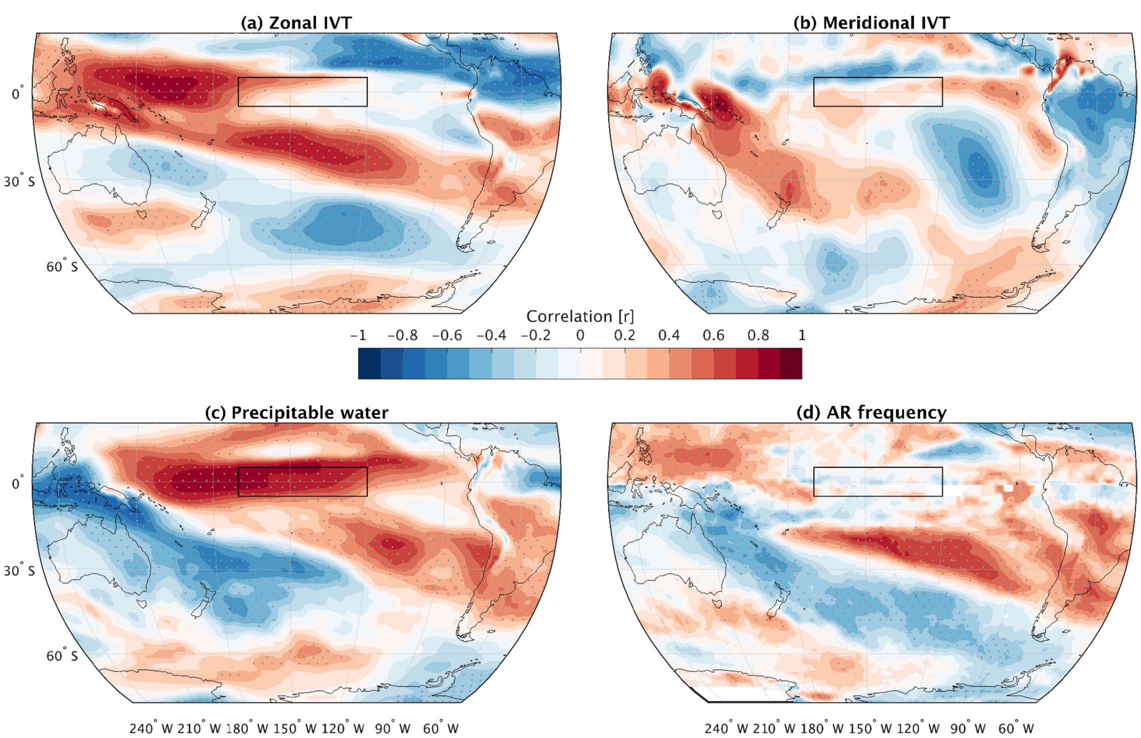

Figure 3: Composite of the interannual correlation (1979-2014) between the ONI index and (a) zonal integrated water vapor transport uIVT, (b) meridional integrated water vapor transport vIVT, (c) PW, and (d) ARs frequency. Shaded area shows statistically significant correlations at the 95% level, according to a Monte Carlo test (n = 10000). Box over the map shows the location of El Niño 3.4 region.

The uIVT and the AR-frequency are more linearly correlated with ONI than with the local (point to point) SST in the subtropical Pacific, between 20-30°S and 180-100°W (Figure S3), which could indicate moisture transport in the South Pacific is controlled by changes in the central equatorial Pacific SST, rather than by local changes of SST. The above suggests that ENSO plays a key role in the variability of moisture transport from the South Pacific to the western coast of South America on an interannual timescale.

During El Niño years, a pattern of upper-level tropospheric anomalies has been associated with the propagation of a quasi-barotropic Rossby wave arising from the shift of anomalous convection in the equatorial Pacific: an anomalous high in the central equatorial Pacific, an anomalous subtropical low, and an anomalous high near the Amundsen-Bellingshausen Sea (black contours in Fig. 4a), consistent with the large-scale teleconnection patterns described as the PSA mode (Karoly, 1989; Mo & Higgins, 1998; Rutllant & Fuenzalida, 1991; Trenberth et al., 1998). In La Niña years, the pattern of anomalies has almost the exact opposite sign (Fig. 7b).

IVT anomalies in the subtropical Southern Pacific tend to follow the circulation of the anomalous subtropical high (centered at around 15°S and 150ºW) and the anomalous subtropical low (centered at around 35°S and 130ºW, Fig. 4a). The maximum IVT anomalies, mainly in its zonal component, occur at the northeastern quadrant of the anomalous subtropical low, with values between 60 and 80 kg $m^{-1}s^{-1}$ of uIVT between 15-30°S and 170°-100°W. Downstream of this maximum in IVT, following the anomalous low-level wind, these significant eastward IVT anomalies (~20 kg $m^{-1}s^{-1}$) reach the South American coast with a slight northerly component.

Horizontal convergence at the 700 hPa surface is observed at the equatorial edge of the subtropical anomalous low, mainly in the exit region of the strengthened jet stream, between 20°-30°S and 120°-90°W. Simultaneously, a maximum of positive PW anomalies (~ 3 kg m^{-2}) associated with a maximum of positive AR frequency anomalies (~ 8-9% of the time) is observed extending towards southern South America, following the IVT flow and favoring a local maximum of significant positive anomalies of PW (~ 1.5 to 2 kg m^{-2}, Fig 4a) and AR-frequency (~ 3-5% of the time, Fig. 4b), in the coast of central-northern Chile.

On the other hand, the ERA-Interim precipitation data show positive anomalies around the subtropical low and negative anomalies in the anomalous polar high; however, the maximum precipitation anomaly (~ +1.5 sigma, in standardized anomalies) occurs off the coast of north-central Chile, coinciding with the maximum of AR-frequency and a minimum of OLR anomalies (~ -10 Wm^{-2}, Fig. 4c), which suggests an increase in cloudiness and enhanced precipitation due orographic processes.

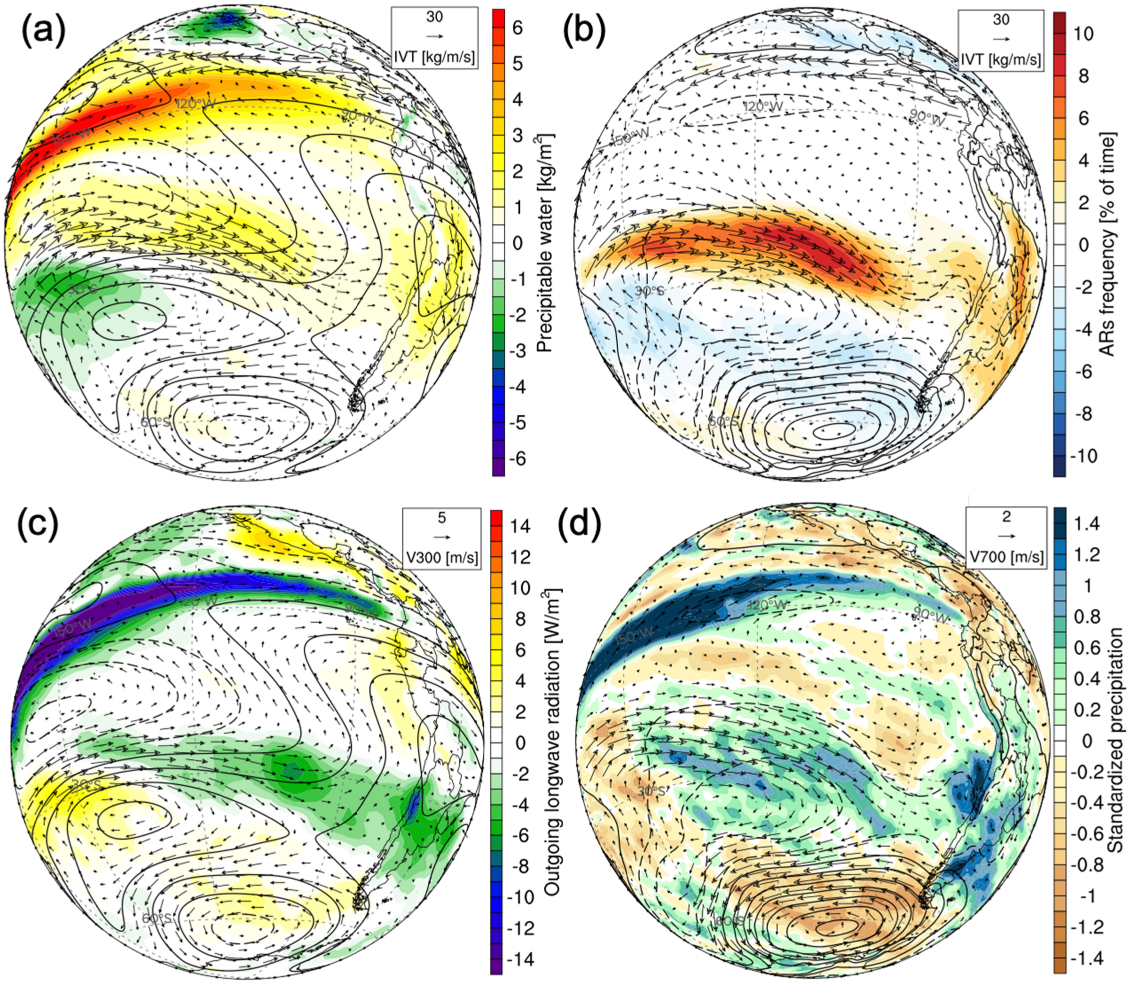

Figure 4: Anomaly composites for the JJA period in El Niño years. (a) 300 hPa Streamfunction in contours (m^2 s^{-1}), IVT in vectors (kg m^{-1} s^{-1}), and PW in colors (kg m^{-2}), (b) as in (a) but mean sea level pressure in contours (hPa) and AR frequency in colors (% of the time), (c) as in (a) but 300 hPa vector wind in vectors (m s^{-1}) and OLR from NOAA Interpolated OLR in colors (W m^{-2}), and (d) as in (b) but 700 hPa vector wind in vectors (m/s), standardized precipitation in colors and sea level pressure (contours). Negative contours in dotted lines.

Using the daily data from the Tahiti, Easter Island, and Santo Domingo radiosondes (see stars in Fig 1a for locations), we can look at some of the evolution of the moisture anomalies in their trajectory towards South America. During El Niño years, the entire daily PW density curve is displaced to the right, increasing the probability of having days with high values of PW. During La Niña, a left displacement is shown. During the warm phase of ENSO, days with values of PW comparable with those at the tropical Pacific Islands (> 20 kg m^{-2}) become more likely at the coast of Central Chile (Fig. 5a). On the other hand, the daily uIVT probability density function exhibits similar behavior; the warm phase of ENSO favors an increase in the probability of high values of positive uIVT in all stations (Fig. 5b-d), consistent with the moisture transport from the equatorial-central Pacific along the "extended" SPCZ towards South America.

In terms of the daily precipitation intensity, the days with precipitation associated with ARs are more intense than those not associated with ARs, especially in the CS and S zones (also documented by Valenzuela & Garreaud, 2019). The probability of exceeding the 75th percentile (p75) of daily precipitation increases from 35% to 44% from north to south during days associated with ARs (figure 6). In the CN zone, a significant increase in the daily precipitation associated with AR is observed during El Niño years —the probability of exceeding the 75th percentile of the daily precipitation distribution increases to 52%. Not only do high values of daily precipitation increase, but rainfall of any amount becomes more likely in El Niño years; the probability function of El Niño-AR is significantly different from La Niña-AR (according to the k-s test with $p = 0.0045$) and significantly different from the curve of all ARs ($p = 0.0069$). In the CS and S zones, El Niño does not have the same impact on the intensity of precipitation associated with AR during wintertime, and the distribution curve changes are not significant (Fig. 6b and 6c).

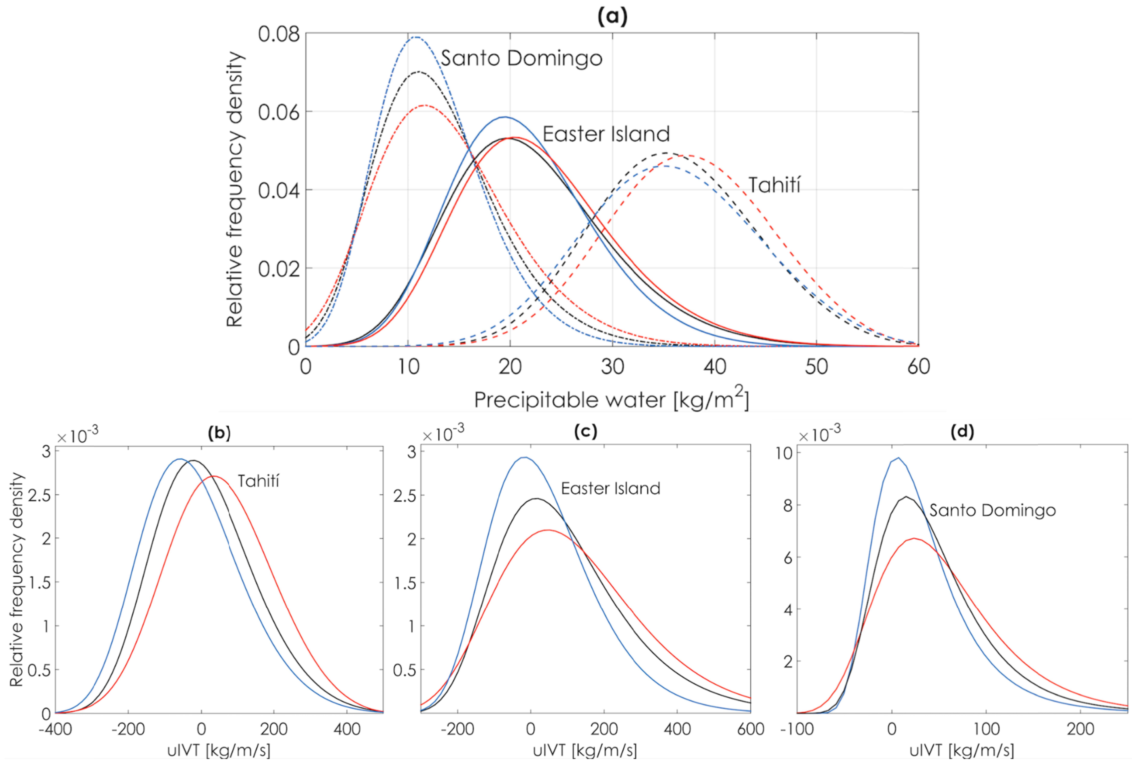

Figure 5: Probability density function PDF of wintertime (JJA) daily data obtained from radiosondes during the period 1981-2010 (black), El Niño years (red), and La Niña years (blue). (a) PW at the three selected launch locations (kg/m2), (b) zonal integrated water vapor transport (uIVT, in kg/m/s) at Tahiti, (c) as in (b) but in Easter Island, and (d) as in (c) but in Santo Domingo. Launching locations are shown in Figure 1a.

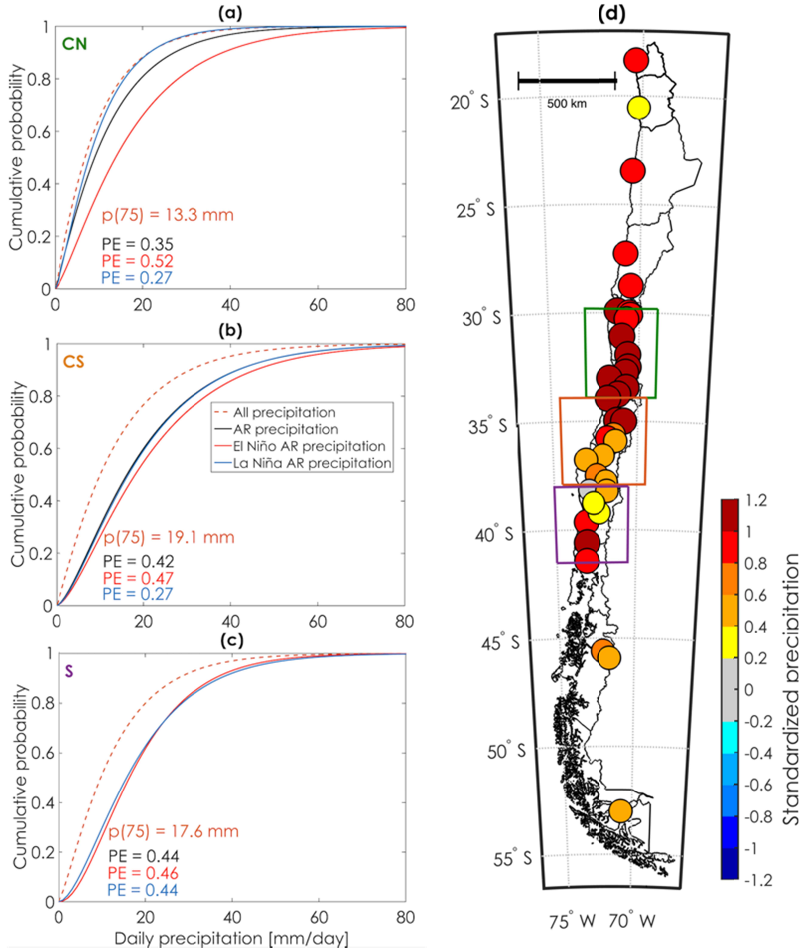

Figure 6: Cumulative probability function (CDF) of the wintertime (JJA, 1979-2014) daily precipitation (mm/day) for the CN region. All days with precipitation are shown in the segmented brown line, days with AR-related precipitation are shown in the black line, and days with AR-related precipitation during El Niño (La Niña) years are shown in the red (blue) line. (b) As in (a) but for the CS region, and (c) as in (b) but for the S region. The AR-related precipitation (black) and La Niña ARs (blue) exhibit the same distribution in the S region. (d) Composite of standardized precipitation anomalies in Chile during El Niño. Panels (a), (b), and (c) show the 75th percentile (p(75)) of the distribution of all precipitation and the probability of exceedance (PE) for each data set.

Table 1: Seasonal (JJA) means and standard deviations for the CN zone. In bold, values significantly different from climatology, according to a Monte Carlo experiment.

Variable	CN Zone		
	Climatology	El Niño	La Niña
AR frequency (% of the time)	9.1 +/- 4.8	**13.5** +/- 6.8	**5.6** +/- 2.8
AR events (#)	8 +/- 3	8 +/- 4	6 +/- 2
AR duration (days)	2.0 +/- 0.7	**2.8** +/- 1.1	**1.6** +/- 0.5
Days with AR (days)	15.6 +/- 7.2	**22.2** +/- 9.8	**10.7** +/- 4.9
AR precipitation (mm/day)	8.2 +/- 5.0	**14.1** +/- 5.3	**5.7** +/- 3.6
AR-precipitation days (days)	8.2 +/- 4	**13.8** +/- 6	**5.5** +/- 2
Accumulated AR-precipitation (mm)	110 +/- 100	**250** +/- 130	**60** +/- 50

During El Niño winters in the CN zone, AR-frequency increases; however, the number of independent AR events does not necessarily increase, so the significant increase in the number of days with AR is produced by an increase in the duration of the events (Table 1). This increase in the number of days is accompanied by a significant increase in the daily precipitation rate and in the number of days with precipitation associated with ARs, which causes a significant increase in winter AR-associated precipitation. In La Niña winters, the opposite occurs, a decrease in the number of days with ARs, which produce lower daily amounts of precipitation, resulting in a decrease in seasonal precipitation associated with ARs.

The differences between El Niño winters and climatology in the CS and S zones are smaller and less significant than those observed in the CN zone. During La Niña winters in the CS zone, the number of days with ARs decreases, with a slight decrease in individual events. The lower number of days with

ARs produces a lower number of AR-precipitation days, which ultimately implies a decrease in the total seasonal AR-associated precipitation. During El Niño years, higher AR-associated precipitation is observed; however, the differences are not significant. In the S zone, the differences between the El Niño and La Niña years with respect to climatology are less than what was observed in the CN and CS zones during winter but exhibit the same behavior (see Table. S1).

4. Discussion

In the previous sections we have discussed the effect of the teleconnection pattern on the moisture transport in the Southern Pacific and the possible role that this transport plays in the increase in precipitation during the warm phase of ENSO in Central Chile (~ 30ºS-38ºS). The anomalies of IVT closely follow the contours of streamfunction along the large-scale Rossby wave train in the Southern Pacific; that is, the maximum IVT along the anomalous subtropical low (identified as an L in Fig. 7a) is also the location of the maximum anomaly of AR frequency during this warm phase. Although we show streamfunction contours to highlight the Rossby wave train in upper levels, anomalies of IVT, mean sea level pressure, and wind at 700 hPa (see Fig. 4d) are nearly colocated, which confirms the quasi-barotropic nature of the Rossby wave response outside the tropics. Therefore, the increased transport of IVT along the corridor between the tropical high and the subtropical low occurs coherently across the depth of the troposphere. This climatological feature has been observed previously associated with an eastward shift of the SPCZ and, simultaneously, a poleward shift of the Pacific ITCZ during the warm phase of ENSO (Garreaud & Battisti, 1999). Even though the SPCZ is not as prominent in the Austral winter as it is in the Austral summer, during the warm phase of ENSO, an eastward extension of the SPCZ (approximately 1000 km) is observed. This is accompanied by a slight reduction in the southeastward inclination when compared to the climatology. During La Niña, the opposite is true; the wintertime SPCZ retracts to the west and becomes less organized (see Figs. 7a and 7b).

From a synoptic scale perspective, during El Niño years, the patterning of water vapor and formation of ARs is enhanced, following the southwesterly flow in between the poleward region of the tropical high and the equatorward region of the subtropical low. The chain of events is likely modulated by the synoptic and intraseasonal forcing, as water vapor is transported episodically through ARs along this moisture corridor. The anomalies weaken as they approach South America, presumably due to the "erosion" of the precipitable water as moisture travels towards the continent, which by necessity implies a reduction in moisture in the marine boundary layer in equilibrium with the colder upwelling waters. Above the boundary layer, where tropical temperatures are homogeneously warmer during El Niño, the decrease in moisture is not as significant. On the other hand, fronts usually display a meridional orientation in part due to the barrier flow near the Andes (Barrett et al., 2009) or even sometimes rotate along the coast, usually progressing toward lower latitudes as the colder and drier air pushes the atmospheric river equatorward. The cold air behind the surface front is a region of extremely dry air, also explaining the decrease of PW near the continent in the climatological sense. Some individual storms can even produce precipitation without the need for the atmospheric river to land over the continent, for instance, in the recent case of 2021, where most of the precipitation occurred after the IVT maximum near the coast, where water vapor was organized by convective instability (Valenzuela et al., 2022). In many cases, water vapor is transported near the continent and further organized by a system that could be different from the original atmospheric river (a cut-off low, for example). Nevertheless, trajectory analyses such as the ones conducted by Langhamer et al. (2018) for Patagonia could clarify fine details of the moisture transport to the continent. In fact, Rutllant et al. (2023) show that for extreme events that lead to landslides in Northern Chile, many of the trajectories originate in the Central Pacific about four days before an AR landfall, near the region identified here as the region of a major increase in westerly IVT between the tropical high and the subtropical low.

Under warmer equatorial central Pacific, enhanced moisture is available for atmospheric rivers reaching the Southern and Central coast of Chile, in fact, ARs do show higher intensities than during the cold phase of ENSO. Given that processes such as convergence and condensation along the atmospheric river are also important, we do not expect water vapor reaching the continent to come entirely from the tropical region (e.g. Dacre et al., 2015). We observe that during the warm phase of ENSO, there is an equatorward shift of the maximum frequency of AR landfall, similar to changes in the frequency of landfall with ENSO for wintertime on the west coast of North America (Mundhenk et al., 2016; Payne & Magnusdottir, 2014).

As we discussed in the introduction, the alternative hypothesis for the increase in precipitation during wintertime in El Niño years is the increase of baroclinic perturbations along the subtropics due to the blocked extratropical flow (Rutllant & Fuenzalida, 1991) and the larger intensity of the subtropical jet, which produces an increase in baroclinic perturbations along subtropical latitudes (Montecinos & Aceituno, 2003). Here, we calculated a simple climatology of such perturbations using the anomalies of daily meridional wind at 500 hPa. A perturbation occurrence in each grid point is defined whenever the northerly daily wind anomaly is higher than 10 m s^{-1}. The resulting climatology of these so-defined perturbations (see Fig. S5) depicts very closely the mean position of both the polar and the subtropical storm tracks compared to other methods available in the literature (Hoskins & Hodges, 2005; Trenberth, 1991). In Fig. 7a and 7b. the colors show anomalies over the 1979-2014 period for El Niño and La Niña.

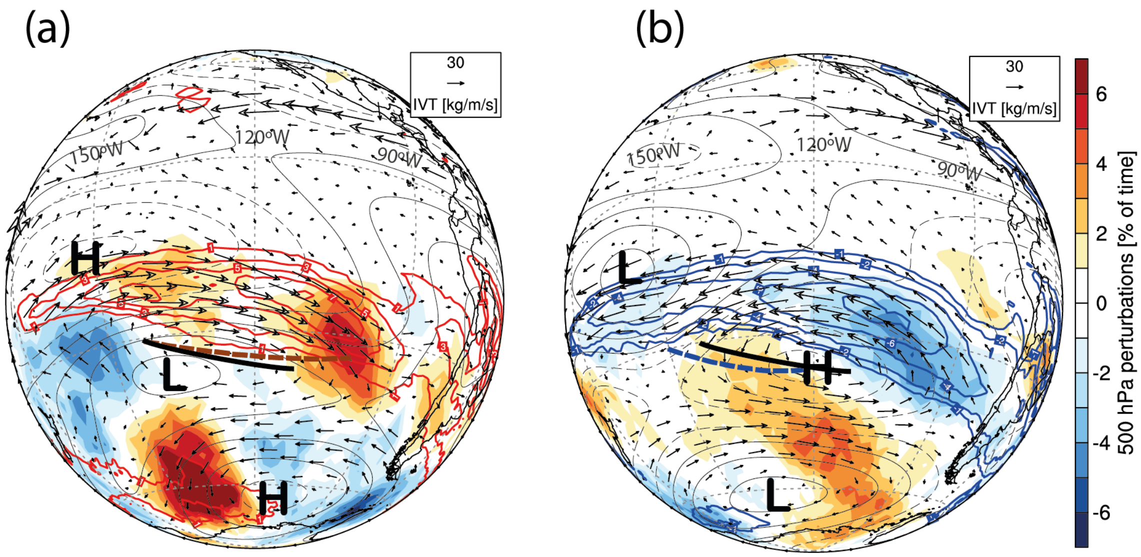

Figure 7: Anomaly composites for the JJA period of 500 hPa perturbations in colors (% of time), 300 hPa streamfunction in contours (in m^2 s^{-1}), IVT in vectors (kg m^{-1} s^{-1}) and AR frequency in colored contours (% of time) in (a) El Niño years (positive contours in red) and (b) La Niña years (negative contours in blue). The location of the SPCZ from GPCP rainfall data is indicated by a solid black line, a red dashed line for the SPCZ during El Niño in panel (a), and a blue dashed line for the SPCZ during La Niña in panel (b). L and H in the figure represent low and high pressure, respectively.

Figure 7a shows that there is indeed an equatorward shift of the subtropical stormtrack during El Niño years and, conversely, a poleward shift during La Niña years. The lower perturbation activity over the Amundsen-Bellingshausen Sea is consistent with the anomalous blocking high during the ENSO warm phase (Rutllant & Fuenzalida, 1991), as described by the "dry-dynamics" explanation The eastern shift of the SPCZ, associated with an increase in moisture transport towards the southeast, seems to favor the increase in ARs in the northeastern quadrant of the subtropical low. We can see that the positive anomalies of perturbations in 500 hPa closely match the positive anomalies in ARs frequency, with a maximum at ~ 30ºS and 105ºW. Local low-level convergence, produced by enhanced baroclinicity in this region, could be the cause of the formation and enhancement of ARs, following the conceptual model described, for instance, by Dacre et al. (2015).

Regarding the relationship between moisture transport and precipitation, we have shown that there is a high correlation at the seasonal scale between IVT and precipitation. The location of the maximum correlation between IVT and precipitation to the north of each of the defined regions is in accordance with previous work that shows the northwest direction of IVT transport is the most favorable to precipitation in Central and Southern Chile. We have also observed an increased frequency, intensity, and duration of Atmospheric Rivers (ARs) during El Niño periods, contrasted with a corresponding decrease during La Niña phases. This aligns with earlier findings of an increase in storm duration during El Niño, irrespective of frequency, as documented by Hernández et al., (2022).

In addition to the diversity within ENSO itself (e.g. Johnson, 2013), non-tropical sources of variability on interannual and longer time scales could interfere with ENSO's precipitation response. For instance, the past decade has seen a sea level pressure dipole with positive anomalies across the subtropical Pacific and negative anomalies at mid-latitudes, similar to a La Niña pattern. This dipole pattern has been linked to the mega-drought in south-central Chile and to a persistent warm SST anomaly in the Southwestern Pacific, known as the 'Southern Blob' (Garreaud et al., 2020, 2021). This interference with the PSA mode, through the Southern Blob, could potentially reduce the correlation between equatorial Pacific SST and precipitation in Central Chile, masking ENSO's influence. Similarly, an emerging signal from global warming has been documented in Central Chile's precipitation patterns over the last few decades (Boisier et al., 2016). Further research is required to understand the interactions between ENSO and these emerging modes of variability. This will help clarify the potential changes that may alter the responses in moisture transport and AR frequency, which we are currently documenting

Finally, we present in Fig. 8 a summary of our understanding of the relation between ENSO and precipitation in Central Chile during wintertime. During the warm phase of ENSO, deep tropical convection shifts towards the Central Pacific from the Western Pacific warm pool. This convection anomaly generates upper-level anomalous divergence and a large-scale Rossby wave response, usually identified as the PSA mode, with a tropical anticyclone southwest of the maximum anomalous convection, a subtropical cyclone and a polar anticyclone over the Amundsen-Bellingshausen sea. Changes in the circulation induced by anomalous tropical heating increase the westerly transport of water vapor in the Western equatorial region as well as in the SPCZ, which extends eastward. In the northeastern quadrant of the subtropical low, integrated water vapor transport is enhanced during the warm ENSO phase. Atmospheric river frequency shows a maximum in the same region, as well as a measure of synoptic scale perturbations in 500 hPa, which we interpret as the poleward shift of the stormtrack in the subtropics associated with the blocking of the extratropical flow in extratropical South America. During the warm phase of El Niño, increased precipitation in Central Chile is associated with more intense, more frequent, and longer-lasting atmospheric rivers. In between the region of maximum AR frequency change and the continent, there is still a gap of about 2000 km, which atmospheric moisture needs to cover. Once the transport along the SPCZ reaches the baroclinic zone in the subtropics, the zonal transport becomes less coherent, due in part to the baroclinic activity in the region; nonetheless, ARs are stronger and longer-lived under these conditions, which results in about a doubling of precipitation in Central Chile due to ARs during the warm ENSO phase.

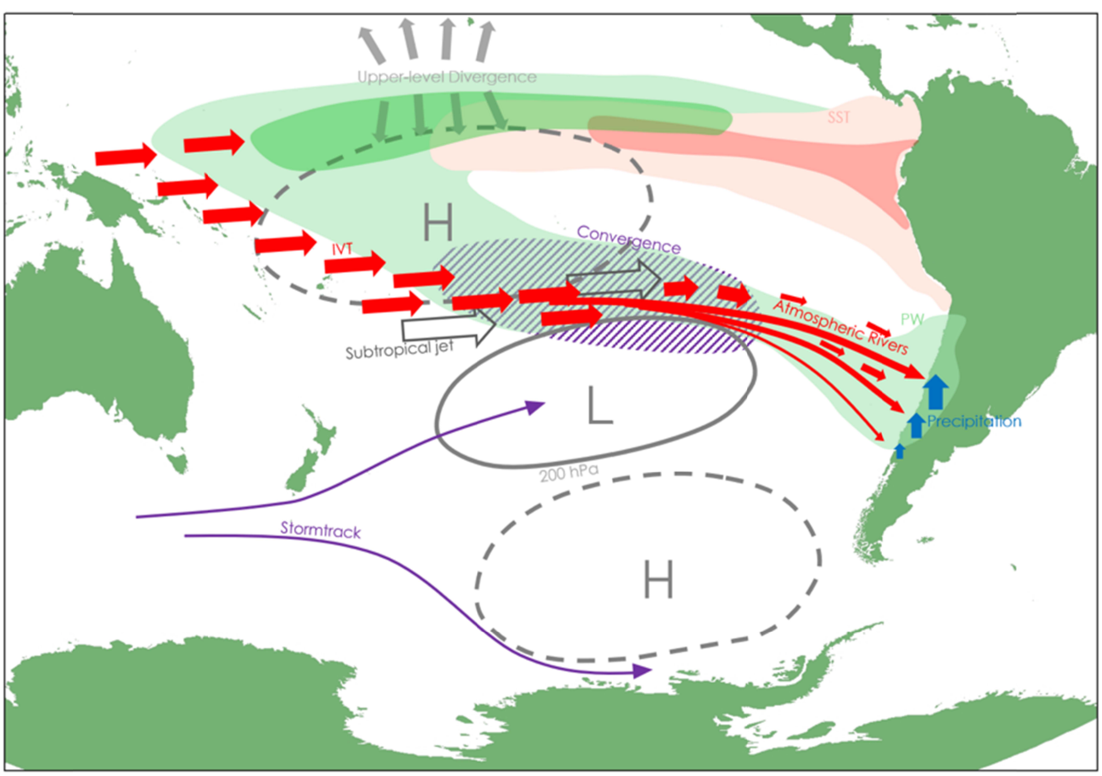

Figure 8: Schematic of the South Pacific response to anomalous heating in the Central Pacific during the wintertime for a positive ENSO phase.

How much water vapor is transported to the continent by the atmospheric rivers in the moist corridor between the tropical high and the subtropical low? This question cannot be answered with the present analysis. A quantitative budget would require calculations of the transport, condensation, evaporation, and convergence of water along each of the atmospheric rivers that occurred over each ENSO phase, or alternatively using a water vapor tracer technique to isolate the tropical/subtropical contribution from the local sources. However, the role of water vapor transported along the atmospheric rivers goes beyond the actual budget of water. For instance, a moister free-troposphere provides a better environment for precipitation than the usually dry free-troposphere associated with the subsidence in the South Eastern Pacific Anticyclone. We could hypothesize that moister systems during the warm ENSO phase, due to larger release of latent heat in the warmer region of the cold front, can be more vigorous and therefore produce stronger cyclogenesis and local convergence of water vapor. These indirect effects can be more important in our region than in other regions of the planet, given the relatively low availability of water vapor due to the cold ocean and the semi-permanent dry free-troposphere warranted by strong subsidence due to the descending Hadley circulation.

Data Availability Statement

The Oceanic El Niño Index can be obtained from the CPC-NOAA website: https://origin.cpc.ncep.noaa.gov/products/analysis_monitoring/ensostuff/ONI_v5.php. ERA-Interim data can be downloaded from the NCAR Research Data Archive: https://rda.ucar.edu/datasets/ds627.0/dataaccess/. The atmospheric river catalog can be obtained from: https://ucla.app.box.com/v/arcatalog/. OLR data can be downloaded from the NOAA Interpolated OLR database: https://psl.noaa.gov/data/gridded/data.olrcdr.interp.html. Weather station data is available from the Dirección Meteorológica de Chile website: https://climatologia.meteochile.gob.cl/. Data from the radiosondes launches can be found at the Wyoming University website: https://weather.uwyo.edu/upperair/sounding.html.

References

Aceituno, P. (1988). On the Functioning of the Southern Oscillation in the South American Sector. Part I: Surface Climate. *Monthly Weather Review*, *116*(3), 505–524.

Aceituno, P., Boisier, J. P., Garreaud, R., Rondanelli, R., & Rutllant, J. A. (2021). Climate and Weather in Chile. *World Water Resources*. https://doi.org/10.1007/978-3-030-56901-3_2

Barrett, B. S., Garreaud, R., & Falvey, M. (2009). Effect of the Andes Cordillera on Precipitation from a Midlatitude Cold Front. *Monthly Weather Review*, *137*(9), 3092–3109.

Boisier, J. P., Rondanelli, R., Garreaud, R. D., and Muñoz, F. (2016), Anthropogenic and natural contributions to the Southeast Pacific precipitation decline and recent megadrought in central Chile, *Geophys. Res. Lett.*, 43, 413– 421, doi:10.1002/2015GL067265.

Carrasco-Escaff, T., Rojas, M., Garreaud, R., Bozkurt, D., & Schaefer, M. (2022). Climatic control of the surface mass balance of the Patagonian Icefields. *EGUsphere*, 1–32.

Dacre, H. F., Clark, P. A., Martinez-Alvarado, O., Stringer, M. A., & Lavers, D. A. (2015). How Do Atmospheric Rivers Form? *Bulletin of the American Meteorological Society*, *96*(8), 1243–1255.

Dee, D. P., Uppala, S. M., Simmons, A. J., Berrisford, P., Poli, P., Kobayashi, S., et al. (2011). The ERA-Interim reanalysis: configuration and performance of the data assimilation system. *Quarterly Journal of the Royal Meteorological Society*, *137*(656), 553–597.

Garreaud, R. D., & Battisti, D. S. (1999). Interannual (ENSO) and interdecadal (ENSO-like) variability in the Southern Hemisphere tropospheric circulation. *Journal of Climate*. Retrieved from https://journals.ametsoc.org/view/journals/clim/12/7/1520-0442_1999_012_2113_ieaiel_2.0.co_2.xml

Garreaud, R. D., Alvarez-Garreton, C., Barichivich, J., Boisier, J. P., Christie, D., Galleguillos, M., et al. (2017). The 2010–2015 megadrought in central Chile: impacts on regional hydroclimate and vegetation. *Hydrology and Earth System Sciences*, *21*(12), 6307–6327.

Garreaud, R. D., Boisier, J. P., Rondanelli, R., Montecinos, A., Sepúlveda, H. H., & Veloso-Aguila, D. (2020). The Central Chile Mega Drought (2010–2018): A climate dynamics perspective. *International Journal of Climatology*, *40*(1), 421–439.

Garreaud, R. D., Clem, K., & Veloso, J. V. (2021). The South Pacific Pressure Trend Dipole and the Southern Blob. *Journal of Climate*, *34*(18), 7661–7676.

Guan, B., & Waliser, D. E. (2015). Detection of atmospheric rivers: Evaluation and application of an algorithm for global studies. *Journal of Geophysical Research, D: Atmospheres*, *120*(24), 12514–12535.

Horel, J. D., & Wallace, J. M. (1981). Planetary-Scale Atmospheric Phenomena Associated with the Southern Oscillation. *Monthly Weather Review*, *109*(4), 813–829.

Hoskins, B. J., & Hodges, K. I. (2005). A New Perspective on Southern Hemisphere Storm Tracks. *Journal of Climate*, *18*(20), 4108–4129.

Johnson, N. C. (2013). How Many ENSO Flavors Can We Distinguish? *Journal of Climate*, *26*(13), 4816–4827.

Karoly, D. J. (1989). Southern hemisphere circulation features associated with El Niño-Southern Oscillation events. *Journal of Climate*, *2*(11), 1239–1252.

Langhamer, L., Sauter, T., & Mayr, G. J. (2018). Lagrangian Detection of Moisture Sources for the Southern Patagonia Icefield (1979–2017). *Frontiers of Earth Science in China*, *6*. https://doi.org/10.3389/feart.2018.00219

L'Heureux, M. L., Collins, D. C., & Hu, Z.-Z. (2013). Linear trends in sea surface temperature of the tropical Pacific Ocean and implications for the El Niño-Southern Oscillation. *Climate Dynamics*, *40*(5), 1223–1236.

Liebmann, B., & Smith, C. A. (1996). Description of a Complete (Interpolated) Outgoing Longwave Radiation Dataset. *Bulletin of the American Meteorological Society*, *77*(6), 1275–1277.

Marques, R. F. C., & Rao, V. B. (1999). A Diagnosis of a Long-Lasting Blocking Event over the Southeast Pacific Ocean. *Monthly Weather Review*, *127*(8), 1761–1776.

Mo, K. C., & Higgins, R. W. (1998). The Pacific-South American modes and tropical convection during the Southern Hemisphere winter. *Monthly Weather Review*, *126*(6), 1581–1596.

Montecinos, A., & Aceituno, P. (2003). Seasonality of the ENSO-related rainfall variability in central Chile and associated circulation anomalies. *Journal of Climate*, *16*(2), 281–296.

Mundhenk, B. D., Barnes, E. A., & Maloney, E. D. (2016). All-Season Climatology and Variability of Atmospheric River Frequencies over the North Pacific. *Journal of Climate*, *29*(13), 4885–4903.

Payne, A. E., & Magnusdottir, G. (2014). Dynamics of landfalling atmospheric rivers over the North Pacific in 30 years of MERRA reanalysis. *Journal of Climate*. Retrieved from https://journals.ametsoc.org/view/journals/clim/27/18/jcli-d-14-00034.1.xml?tab_body=pdf

Pittock, A. B. (1980). Patterns of Climatic Variation in Argentina and Chile—II. Temperature, 1931–60. *Monthly Weather Review*, *108*(9), 1362–1369.

Quinn, & Neal. (1983). EL NIÑO, AND CHILEAN SUBTROPICAL RAINFALL. *Fishery Bulletin* . Retrieved from https://books.google.com/books?hl=es&lr=&id=Thp5UFGVfzsC&oi=fnd&pg=PA363&dq=quinn+and+neal+&ots=lYfi6xEVnM&sig=4fA82JM-wjor1fpFtGafndhu1yo

Rubin, M. J. (1955). An analysis of pressure anomalies in the Southern Hemisphere. Notos.

Rutllant, J. (2004). Aspectos de la circulación atmosférica de gran escala asociada al ciclo ENOS 1997-1999 y sus consecuencias en el régimen de precipitación en Chile central. In S. A. J. C. J. Rutllant y Yañez (Ed.), *El Niño-La Niña 1997-2000. Sus Efectos en Chile* (pp. 61–76).

Rutllant, J., & Fuenzalida, H. (1991). Synoptic aspects of the central Chile rainfall variability associated with the Southern Oscillation. *International Journal of Climatology*, *11*(1), 63–76.

Rutllant, J., Matus, F., Rudloff, V., & Rondanelli, R. (2023). The role of atmospheric rivers in rainfall-induced landslides: A study from the Elqui valley. *Journal of Arid Environments*.

Saavedra, F., Cortés, G., Viale, M., Margulis, S., & McPhee, J. (2020). Atmospheric Rivers Contribution to the Snow Accumulation Over the Southern Andes (26.5° S–37.5° S). *Frontiers of Earth Science* , *8*. https://doi.org/10.3389/feart.2020.00261

Trenberth, K. E. (1991). Storm Tracks in the Southern Hemisphere. *Journal of the Atmospheric Sciences*, *48*(19), 2159–2178.

Trenberth, K. E., Branstator, G. W., Karoly, D., Kumar, A., Lau, N.-C., & Ropelewski, C. (1998).

Progress during TOGA in understanding and modeling global teleconnections associated with tropical sea surface temperatures. *Journal of Geophysical Research, C: Oceans*, *103*(C7), 14291–14324.

Valenzuela, R., & Garreaud, R. D. (2019). Extreme Daily Rainfall in Central-Southern Chile and Its Relationship with Low-Level Horizontal Water Vapor Fluxes. *Journal of Hydrometeorology*, *20*(9), 1829–1850.

Valenzuela, R., Garreaud, R., Vergara, I., Campos, D., Viale, M., & Rondanelli, R. (2022). An extraordinary dry season precipitation event in the subtropical Andes: Drivers, impacts and predictability. *Weather and Climate Extremes*, *37*, 100472.

Viale, M., Valenzuela, R., Garreaud, R. D., & Martin Ralph, F. (2018). Impacts of Atmospheric Rivers on Precipitation in Southern South America. *Journal of Hydrometeorology*, *19*(10), 1671–1687.

Vincent, D. G. (1994). The South Pacific Convergence Zone (SPCZ): A Review. *Monthly Weather Review*, *122*(9), 1949–1970.